Catalytic Roles of Divalent Metal Ions in Phosphoryl Transfer by *Eco*RV Endonuclease†

My D. Sam and John J. Perona*

Department of Chemistry and Interdepartmental Program in Biochemistry and Molecular Biology, University of California at Santa Barbara, Santa Barbara, California 93106-9510

Received January 22, 1999; Revised Manuscript Received April 2, 1999

ABSTRACT: The rate constant for the phosphoryl transfer step in site-specific DNA cleavage by *Eco*RV endonuclease has been determined as a function of pH and identity of the required divalent metal ion cofactor, for both wild-type and T93A mutant enzymes. These measurements show bell-shaped pH−rate curves for each enzyme in the presence of Mg^{2+} as a cofactor, indicating general base catalysis for the nucleophilic attack of hydroxide ion on the scissile phosphate, and general acid catalysis for protonation of the leaving 3′-O anion. The kinetic data support a model for phosphoryl transfer based on wild-type and T93A cocrystal structures, in which the ionizations of two distinct metal-ligated waters respectively generate the attacking hydroxide ion and the proton for donation to the leaving group. The model concurs with recent observations of two metal ions bound in the active sites of the type II restriction endonucleases *Bam*HI and *Bgl*I, suggesting the possibility of a similar catalytic mechanism functioning in many or all members of this enzyme family.

The phosphoryl transfer reactions catalyzed by homodimeric type II restriction endonucleases involve the attack of hydroxide ion on specific phosphates located within a 4−8 bp dyad-symmetric duplex DNA recognition site (*1*, *2*). As appears to be the case for all enzyme-catalyzed reactions on phosphodiesters, phosphoryl transfer proceeds through a trigonal bipyramidal phosphorane transition state (*3*). For both *Eco*RI and *Eco*RV endonucleases, it has been shown via the use of isotopically labeled phosphorothioates that the reaction occurs with inversion of configuration (*4*, *5*). This provides strong evidence for an in-line attack by hydroxide and departure of the 3′-oxygen from apical positions of the trigonal bipyramid. A 5′-phosphorylated oligodeoxynucleotide is generated as the second product. It is very likely that this stereochemical mechanism holds for all enzymes in the family.

*Eco*RV endonuclease has emerged as the best-studied type II restriction enzyme, and is thus a lead system for the exploration of common themes relating to the catalytic mechanism and the origins of the extraordinary specificity. *Eco*RV cleaves the target site GATATC in a blunt-ended fashion at the center TA step (*6*). In company with other members of the family, it exhibits an absolute requirement for divalent metal ions. Each of the three cations (Mg^{2+}, Mn^{2+}, and Co^{2+}) supports activity at high levels, with Mg^{2+} preferred (*7*, *8*). Strong evidence implicating at least two metal ions in catalysis has been obtained from stopped-flow fluorescence studies and from metal-reconstitution experiments (*8*, *9*).

High-resolution X-ray structures of *Eco*RV are available in the unliganded and DNA-bound states in a variety of crystal lattices (*10*−*16*; N. C. Horton and J. J. Perona, submitted for publication). These structures show that the DNA is sharply bent by approximately 50° into the major groove at the center TA step of the recognition site. Bending of the DNA is required for positioning the scissile phosphates adjacent to the important carboxylates of Asp90 and Asp74 in each of the two active sites. One divalent metal ion has been observed bridging the *pro*-S_P scissile phosphate oxygen with these two carboxylates [90/74 site, Figure 1A (*11*, *12*, *16*)]. This metal is positioned to stabilize the incipient negative charge in the pentacovalent transition state. In addition, a water molecule bound in the inner sphere hydrogen-bonds to the 3′-oxygen, suggesting that its metal-activated ionization may be the origin of the proton donated to the leaving group. Mutational analysis of Asp90, Asp74, and the conserved Lys92 in the active site supports essential roles for these three residues in catalysis (*17*).

Early work with *Eco*RV did not produce a convincing candidate for the catalytic base required to generate the attacking hydroxide ion. Phosphorothioate substitution experiments led to the proposal that the adjacent 3′-phosphate might abstract the proton (*18*), but the large required elevation in the pK_a of this group appears to be implausible in view of the known active-site structure. Two other proposed schemes (*8*, *11*) bear resemblance to the two-metal mechanism that is operative in the 3′−5′ exonuclease active sites of *Escherichia coli* DNA polymerase I and T4 DNA polymerase, and in *E. coli* alkaline phosphatase (*19*−*21*). However, these schemes require considerable rearrangements of the DNA relative to what is observed in all crystal structures, to properly juxtapose the scissile P−O bond adjacent to metal ions bound at the 90/74 site and a second

† Supported by National Institutes of Health Grant GM53763 and American Chemical Society Petroleum Research Fund Grant 33381-AC4 (to J.J.P.).

* To whom correspondence should be addressed: Department of Chemistry, University of California at Santa Barbara, Santa Barbara, CA 93106-9510. Telephone: (805) 893-7389. Fax: (805) 893-4120.

10.1021/bi9901580 CCC: $18.00
Published on Web 04/29/1999

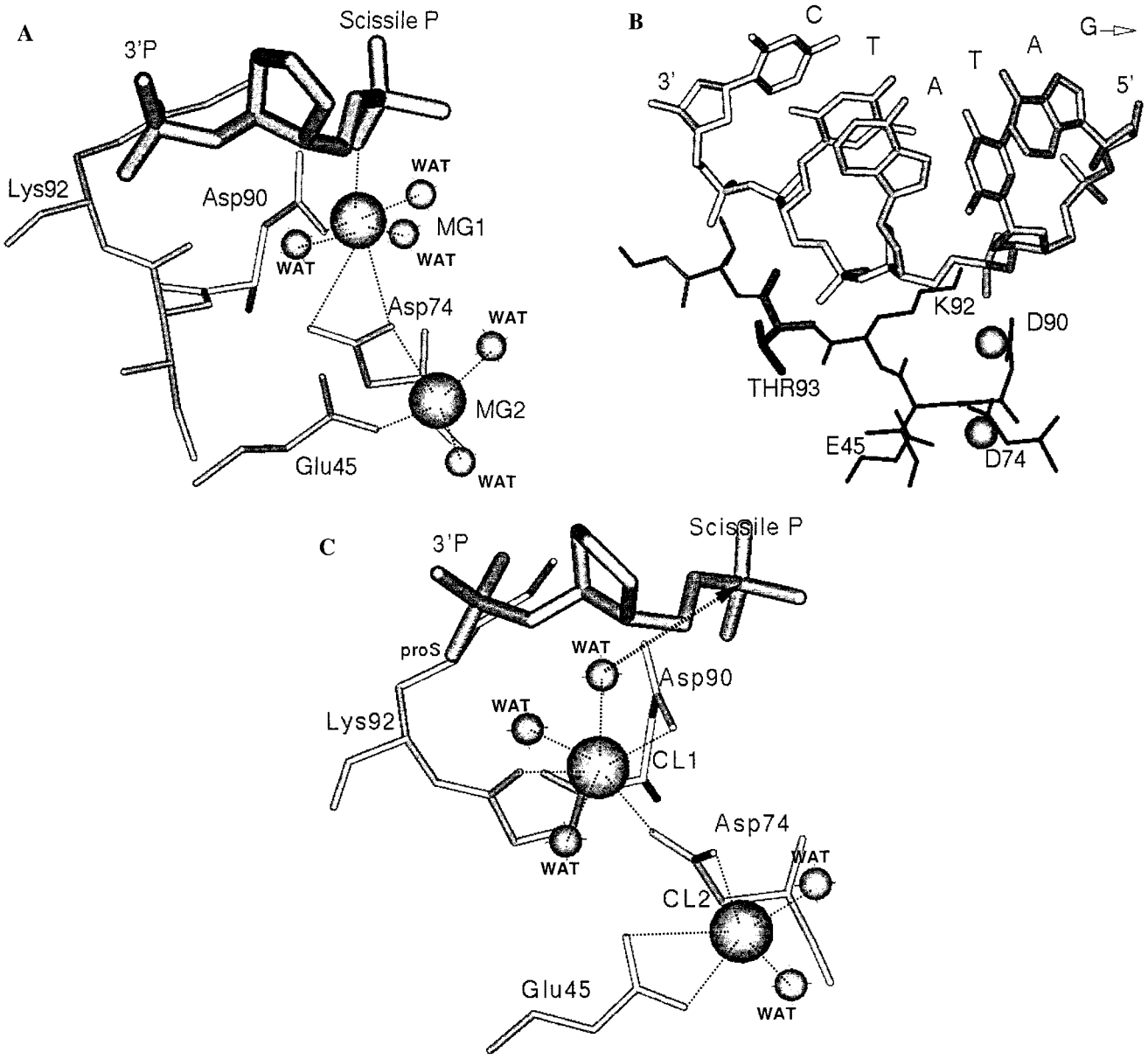

FIGURE 1: Structure of the metal binding sites in the *Eco*RV−DNA complex. (A) Structure and inner sphere ligands in one subunit of the *Eco*RV−DNA−Mg^{2+} complex, visualized by soaking Mg^{2+} into preformed crystals of the protein−DNA complex (*11*). Dotted lines represent inner sphere ligands of the metal ions. (B) View of the DNA conformation spanning the entire GATATC target site, bound to *Eco*RV and Mg^{2+} ions, showing also the location of Thr93 adjacent but not directly within the catalytic site. Spheres denote Mg^{2+} ions. (C) Structure and inner sphere ligands in one subunit of the T93A *Eco*RV−DNA−Ca^{2+} complex, visualized by cocrystallization of the mutant ternary complex (*15*). Note that MG2 (A) and CL2 (C) occupy approximately the same site (74/45 site), but that the sites for MG1 in panel A and CL1 in panel C are distinct. The model for catalysis (*15*) invokes all three of the metals (CL1, MG1, and CL2/MG2), and thus is derived from combining the information from the two separate crystal structures. The arrow in panel C denotes the proposed nucleophilic attack from the inner sphere water of CL1 visualized in the T93A mutant cocrystal structure.

site bridging Asp74 and Glu45 [74/45 site, Figure 1A (*11*)]. Further, neither of these two mechanisms provides a detailed description of the precise roles of the metal ions.

Recently, we located a new divalent metal site in the cocrystal structure of *Eco*RV mutant T93A bound to DNA and Ca^{2+} ions (Ca^{2+} supports specific binding but not catalysis; *15*, *22*). Thr93 lies in the DNA-binding cleft near the adjacent 3′-phosphate at GATApTC (Figure 1B). The hydrated Ca^{2+} ion bound in the new site bridges through a water molecule to the *pro*-S_P oxygen of the 3′-adjacent phosphate, and ligates a second water which is located approximately in-line for attack on the scissile phosphate (Figure 1C). A model of the pre-transition state configuration was constructed by combining information from the wild-type and T93A structures, in which the metal in the new site functions to generate the hydroxide ion nucleophile. To test this model, we have now performed a detailed pH−rate study of both the wild-type and T93A mutant enzymes with Mg^{2+} and Mn^{2+} cofactors. The rate of phosphoryl transfer has been directly measured by single-turnover kinetics, which isolates the chemical step of the reaction and avoids ambiguities associated with pH studies carried out by steady-state methods (*23*). The data reveal bell-shaped curves indicating acid−base catalysis for both wild-type and T93A enzymes with Mg^{2+} as a cofactor. Titrations on the acidic and basic limbs of the profile are interpreted in structural terms, in a manner consistent with the proposed mechanism of phosphoryl transfer (*15*).

MATERIALS AND METHODS

Materials. DNA oligonucleotides were purchased from Integrated DNA Technologies, Inc., and from Midland Certified Reagent Company. T4 polynucleotide kinase was purchased from New England Biolabs. [γ-^{32}P]ATP (6000 Ci/mmol) was purchased from Amersham.

Enzyme Purifications. Wild-type and T93A *Eco*RV enzymes were expressed in *E. coli* from plasmid *p*BSRV (*24*, *25*) and purified to homogeneity by a two-column procedure, as described previously (*12*, *15*, *26*). Purified enzyme preparations were dialyzed into 10% (v/v) glycerol, 0.4 M NaCl, 20 mM potassium phosphate (pH 7.3), and 1 mM DTT, followed by concentration with an Amicon ultrafiltration cell to a concentration of approximately 1.0 mg/mL. Aliquots were then flash-frozen and stored at −70 °C.

Preparation of DNA Substrates. The non-self-complementary 16-mer oligodeoxynucleotide substrate utilized in all assays possesses the sequence 5′-GGGAAAGATATCT-TGG (*16*). This DNA strand and its complement were each purified on a Rainin Pure DNA reverse phase HPLC column, as described previously (*27*). The DNA peak was collected manually, lyophilized, redissolved in TE buffer [10 mM Tris (pH 8.0) and 1 mM EDTA], precipitated with ethanol, relyophilized, and stored as dry pellets at −20 °C. Individual pellets were then redissolved in TE buffer and 5′-end labeled with T4 polynucleotide kinase and [γ-^{32}P]ATP. The excess ATP was removed using Bio-gel P-6 spin columns (Bio-Rad), and the two strands then annealed at various apparent molar ratios and run on nondenaturing polyacrylamide gels. Annealing reactions which produced 95% or more double-stranded DNA were used in the assays. Duplex DNA from different annealing reactions thus contained differing amounts of residual single-stranded DNA, but control experiments in which the amount of single-stranded contamination was deliberately varied gave no differences in measured dissociation constants or cleavage rates. The melting temperature of this duplex substrate is 51 °C (*16*).

Gel Shift Assays. Thermodynamic dissociation constants were obtained by gel electrophoretic mobility shift assays. Assays in the presence of the inactive cofactor analogue Ca^{2+} were performed as described previously (*16*). Binding assays were also performed in the absence of divalent metal. For these assays *Eco*RV and DNA were equilibrated in a binding buffer containing 10 mM bis-tris propane (pH 7.0), 100 mM NaCl, 1 mM EDTA, 0.05 mg/mL BSA, and 3% glycerol. Concentrations of DNA were maintained at least 100-fold below the K_d. The reaction mixtures were incubated for 30 min at ambient temperature (approximately 22 °C) before being loaded onto 12% native polyacrylamide gels running at 200 mV. Immediately after the samples were loaded, the voltage was reduced to 80 mV and the gel run for 1.5 h. The gel running buffer consisted of 20 mM $NaPO_4$ (pH 6.2) and 20 mM KOAc; the pH is shifted to 6.2 to prevent the 16-mer duplexes from dissociating in the gel (*28*). To establish whether this shift in the pH of the diagnostic gel affects the measured equilibrium constant, we used the 22-mer duplex 5′-CTCTTGCGGGATATCGTCCATT as a control sequence. The K_d of this substrate is known (*29*), and we confirmed that for this longer sequence no dissociation occurs in the gel at pH 7.0. Reaction mixtures of wild-type *Eco*RV with this 22-mer substrate were incubated at pH 7.0 and run on parallel gels at pH 7.0 and 6.2. Identical values of 5×10^{-10} M were obtained, as previously determined (*29*). For all reaction mixtures, shifted and unshifted bands were visualized by autoradiography performed with the Storm 840 phosphorimager (Molecular Dynamics). Equilibrium dissociation constants were determined by fitting the data to a standard hyperbolic curve.

Single-Turnover Cleavage Assays. Cleavage at the *Eco*RV site was assayed at 37 °C under conditions of a 3-fold molar enzyme excess over 5′-end-labeled DNA, saturating concentrations of DNA, and varying concentrations of Mg^{2+} and Mn^{2+}. The 16-mer duplex substrate 5′-GGGAAAGATATCT-TGG has the target site located off-center and produces 9-mer and 7-mer single-stranded products. Fast reactions were measured using a rapid quench kinetics apparatus (Kintek RQF-3). For all measurements on the rapid-quench instrument, one sample loop contained DNA and metal ions in a solution containing 50 mM buffer at varying pH, varying concentrations of NaCl (see below), 0.2 mg/mL BSA, and 1 mM DTT. The second loop contained enzyme and metal ions in the same buffer. Control experiments established that inclusion of metal ions with the DNA alone gave identical rates. Mixing the enzyme−DNA complex without divalent metal ions in one syringe, with $MgCl_2$ in the second syringe, gave slower rates as has also been observed in stopped-flow fluorescence experiments (*9*). Other data from this previous study also showed that the binding steps are very fast in comparison with cleavage and product release.

Reactions were initiated by driving the contents of the two sample loops into a single reaction loop. Ten time points were taken for each reaction. Each reaction time point was quenched with a solution containing 4 M urea and 75 mM EDTA. The final collected volume of the reactions was approximately 190 μL. Aliquots (10 μL) from each time point were then mixed with an additional 8−10 μL of quench solution containing bromphenol blue dye. Slower reactions were sampled by hand and were initiated by mixing solutions of enzyme and DNA, each of which contained the divalent metal ion cofactor. Gels were run in a buffer consisting of 50 mM Tris base (pH 8.0), 50 mM boric acid, and 0.33 mM disodium EDTA, at a voltage of 400 mV for 2 h. Substrate and product bands were visualized by autoradiography performed with the Storm 840 phosphorimager (Molecular Dynamics). Reaction rates were fit to a first-order exponential equation. No significant difference in cleavage rate was detected for the two separate strands of the duplex DNA for any reaction.

pH−Rate Profiles. A two-buffer system consisting of bis-tris and bis-tris propane was used for measurements between pH 6.0 and 9.5. Reactions carried out above pH 9.5 were performed in Ches buffer. Equivalent reactions carried out at pH 9.0 in both Ches buffer and the bis-tris/bis-tris propane system gave identical reaction rates. The ionic strength was measured with a conductivity meter at each pH increment and adjusted to a final constant value of 140 mM for all reactions by the addition of NaCl. At pH 7.5, it is known that the enzyme remains fully active for 120 h during reactions performed at 37 °C (*16*). Similar tests were carried out to ensure that activity is not lost during long reactions at pH 6.0 and 10.0, the two extremes of the study described here. Both *Eco*RV and *Eco*RV T93A were incubated at pH 6.0 and 10.0 in the presence of Mg^{2+} or Mn^{2+} for the longest

Table 1: Equilibrium Dissociation Constants and Cleavage Rates

	K_d (M)		k_2 (s^{-1})[a]	
enzyme	with Ca^{2+}	no metal	with Mg^{2+}	with Mn^{2+}
wild-type	$(1.2 \pm 0.5) \times 10^{-13}$ [b]	$(1.9 \pm 0.6) \times 10^{-9}$	0.30 ± 0.01	1.27 ± 0.07
T93A	$(1.1 \pm 2.3) \times 10^{-10}$	$(1.6 \pm 0.2) \times 10^{-8}$	0.0018 ± 0.00015	0.025 ± 0.007

[a] Values of k_2 are those measured at pH 7.0 and are also plotted in Figure 5. The errors are derived in most cases from two independent measurements. The mean value is reported, and the error indicates the difference between the mean and each of the two measurements. Error bars for measurements taken three or more times represent the standard deviation from the mean. The kinetic scheme for duplex DNA cleavage by *Eco*RV (E) is depicted below. S and P represent the intact and cleaved duplexes, and k_2 is the rate constant for cleavage of either single strand. M^{2+} represents two or more divalent metal ions: $E + S + M^{2+}$ (k_1)$\rightleftarrows$(k_{-1}) $E{\cdot}S{\cdot}M^{2+}$ (k_2)$\rightarrow$ $E{\cdot}P{\cdot}M^{2+}$ (k_3)$\rightarrow$ $E + P + M^{2+}$. [b] From Martin et al. (*16*).

time periods required to perform single-turnover reactions at these pHs. Aliquots were then removed from the separate Mg^{2+} and Mn^{2+} incubations and added to reaction tubes containing DNA at pH 8.0. Reaction rates were identical to those of control reactions in which freshly thawed enzymes were directly used at pH 8.0. This establishes that there are no irreversible losses of activity at either of the extreme pH values used in the study. Further control reactions were also performed to ensure saturation of DNA and of divalent metal ions (see Results).

The pH dependencies of the cleavage rate constant (k_2) for reactions carried out with the Mg^{2+} cofactor were fit to eqs 1 and 2, which assume two titratable groups on the enzyme, giving bell-shaped curves with maxima at pH = (pK_{a1} + pK_{a2})/2:

$$k_2 = \frac{K_{max}}{1 + \frac{10^{-pH}}{10^{-pK_{a1}}} + \frac{10^{-pK_{a2}}}{10^{-pH}}} \quad (1)$$

$$k_2 = \frac{K_{max}}{1 + \frac{10^{-pH}}{10^{-pK_{a1}}} + \frac{10^{-pK_{a2}}}{10^{-pH}} + \frac{10^{-pK_{a2}}}{10^{-pK_{a1}}}} \quad (2)$$

where K_{max} represents the maximum value of the titration for each of the single ionizations, pK_{a1} is the pK_a value of the group which is deprotonated (on the acidic limb), and pK_{a2} is the pK_a value of the group which is protonated (on the basic limb) (*30*−*32*). In the case of eq 1, pK_{a1} and pK_{a2} represent "apparent" pK_a values, and in eq 2, these terms represent "true" pK_a values (*31*, *32*). The distinction between these equations becomes insignificant when the two ionizations are greater than one pH unit apart. The program Scientist was used to fit the data.

RESULTS

Structural perturbation approaches can provide considerable insight into enzyme reaction mechanisms. Important considerations in the use of these methods, however, are the extent to which mechanism and structure are conserved in the altered complex. We are employing the T93A mutant of *Eco*RV endonuclease as a probe to elucidate the relationship between conformational changes, metal binding, and formation of a catalytically competent pre-transition state enzyme−DNA−metal ion ternary complex. Thr93 is located in the DNA-binding cleft near the 3′-adjacent phosphate, which is known from phosphorothioate substitution studies to play an important role in catalysis (Figure 1B; *18*). Mutation of Thr93 to Ala perturbs the active-site structure by displacing enzyme and DNA groups by roughly 1 Å, without altering the local conformation of either macromolecule (*15*). The Mg^{2+}-dependent overall activity of *Eco*RV T93A, as measured by k_{cat}/K_m toward a short oligodeoxynucleotide substrate, is 7% of that of the wild-type enzyme (*25*, *33*). Here we relate the pH dependencies of the phosphoryl transfer step in both wild-type and T93A enzymes to the proposed structural mechanism. This mechanism has been derived by combining detailed descriptions of divalent metal ion binding sites from separate high-resolution wild-type and T93A cocrystal structures (Figure 1; *15*).

Equilibrium Binding Constants. To establish the concentrations of DNA required for saturation of the enzyme binding site, thermodynamic dissociation constants were determined for wild-type *Eco*RV and for the T93A mutant by gel mobility shift analysis. The analyses were performed for each enzyme both by omitting the divalent metal cofactor and by substituting the inactive Ca^{2+} cation for Mg^{2+} (*22*). The K_d values for the T93A mutant in the presence of Ca^{2+}, and for both enzymes in the absence of metal, were determined by direct gel shift analysis. The K_d for wild-type *Eco*RV in the presence of Ca^{2+} was determined by equilibrium competition (*16*).

The binding affinity of the 16-mer cognate duplex DNA substrate for T93A is weakened relative to that of the wild type (Table 1). In the absence of metal at pH 7.0, T93A binds DNA approximately 8-fold weaker than does wild-type *Eco*RV. In the presence of Ca^{2+}, however, a much stronger discrimination of 900-fold is observed. Because Ca^{2+} enhances discrimination relative to the condition where divalent metal is absent, it appears likely to provide a good analogue for the enzyme−DNA binding reaction in the presence of an active cofactor. In fact, we have shown that Ca^{2+} quantitatively mimics the performance of Mg^{2+} in providing nearly identical dissociation constants, as measured by comparative gel shift analyses for slowly cleaved complexes containing DNA base analogue substitutions (*44*). *Eco*RV and other restriction enzymes possess acidic side chains adjacent to the scissile phosphates of the DNA, suggesting that electrostatic shielding is an important function of the required divalent cation (*34*). This provides a molecular mechanism explaining why Ca^{2+} enhances binding selectivity. Gel shift analysis of T93A toward a 382 bp DNA fragment in the presence of Ca^{2+} showed a 200-fold reduction in the binding affinity relative to that of the wild type (*33*), similar to the 900-fold effect observed here with short duplexes (Table 1). However, the apparent affinities are 10^3-fold weaker toward the large substrate, because of the presence of nonspecific DNA.

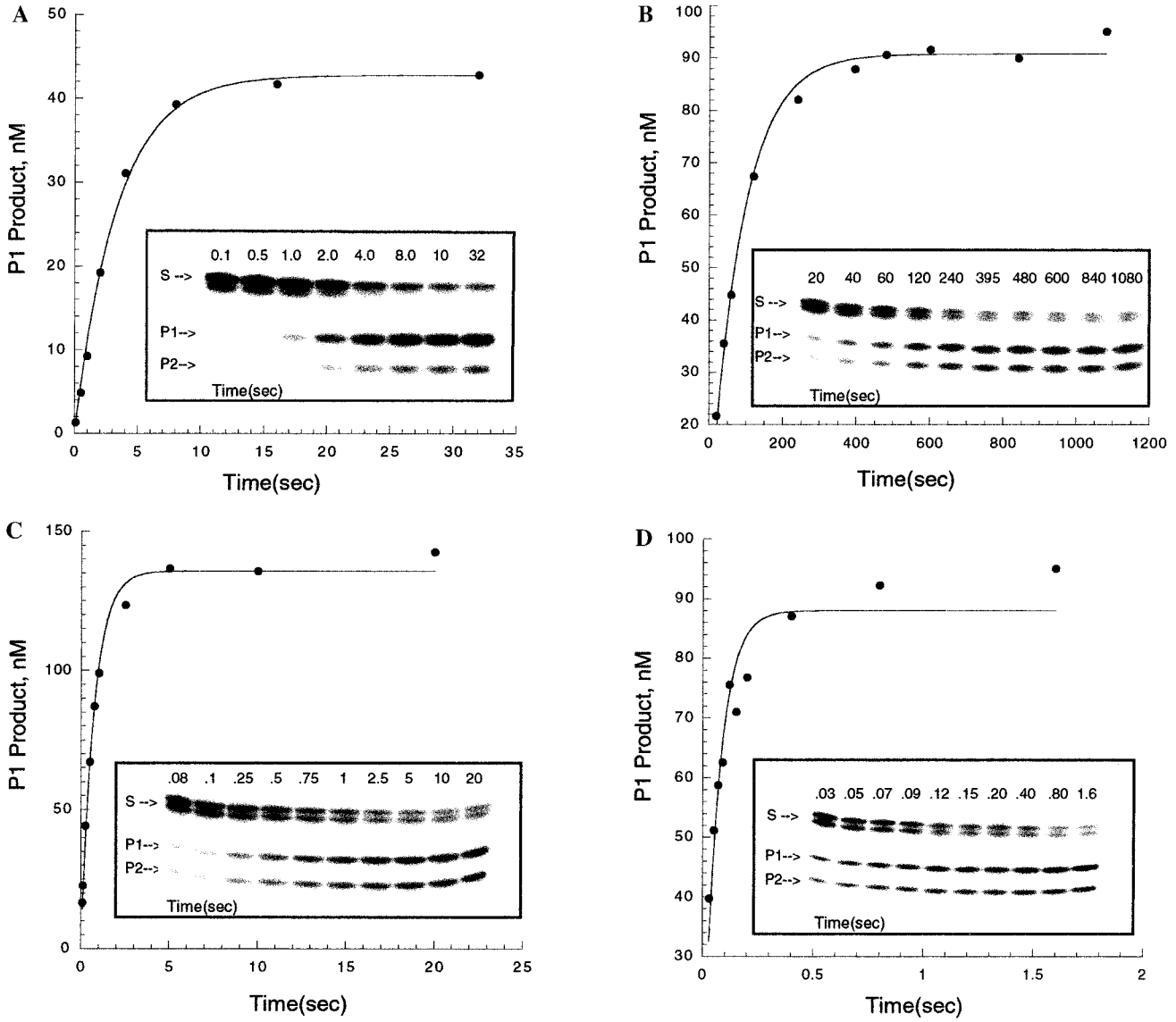

FIGURE 2: Single-turnover reactions with data analysis for the determination of single-turnover cleavage rate constants. The two substrate strands are slightly separated on the denaturing gel because of differences in sequence (one strand is purine-rich and its complement is pyrimidine-rich). The separation of the 9-mer (P1) and 7-mer (P2) products is evident. The reactions shown are (A) wild-type enzyme at pH 7.0 with the Mg^{2+} cofactor, (B) T93A at pH 10.0 with the Mg^{2+} cofactor, (C) T93A at pH 9.0 with the Mn^{2+} cofactor, and (D) wild-type enzyme at pH 9.25 with the Mn^{2+} cofactor.

pH Dependencies of the Chemical Step. Single-turnover reactions with enzyme in 3-fold molar excess of DNA were used to directly measure the rate of the cleavage step of the reaction (Figure 2). The weaker binding affinities in the absence of metal ions (Table 1) were used as a guide in choosing appropriate concentrations. Reactions of wild-type *Eco*RV were assessed at 50 nM DNA and 150 nM enzyme (25-fold above the K_d), while reactions of T93A were assessed at 150 nM DNA and 450 nM enzyme (10-fold above the K_d). Because the affinity of *Eco*RV for DNA in the absence of metal ions decreases with increasing pH (*29*), the dependence of the cleavage rate on the total concentration of the enzyme−DNA complex was further evaluated at pH 10.0 (Mg^{2+} reactions) and 9.0 (Mn^{2+} reactions). At these pH values, the concentrations of DNA and wild-type enzyme were each increased by 3-fold and the cleavage rates remeasured. Rates were found to be identical (data not shown), indicating saturation at alkaline pH as well.

Titrations of Mg^{2+} and Mn^{2+} concentrations were performed for both wild-type and T93A reactions, at pH 6.5 (Mn^{2+}) or 7.0 (Mg^{2+}) (Figure 3). It is evident that Mn^{2+} binds to the wild-type enzyme−DNA complex more tightly than does Mg^{2+}, with saturation being observed at approximately 2.5 mM $MnCl_2$ and 10 mM $MgCl_2$. These concentrations of Mn^{2+} and Mg^{2+} are also saturating for T93A, which binds the metal ions with apparent affinities that are equal to or greater than that of wild-type *Eco*RV. A higher affinity of the wild-type enzyme for Mn^{2+} ions has also been found for plasmid substrates (*7*). Importantly, both the Mg^{2+} and Mn^{2+} titrations display plateaus in activity for both enzymes, providing good evidence for metal ion saturation. At higher concentrations of either metal ion, the activities decrease somewhat. This may indicate the presence of additional weaker-binding inhibitory sites which become occupied at very high metal ion concentrations. All measurements of the pH dependencies of the cleavage rates were carried out at the saturation concentrations of divalent metal. Elevations of the metal chloride concentrations at pH 10.0 (to 15 mM $MgCl_2$) and 9.0 (to 5 mM $MnCl_2$) gave very small cleavage rate decreases, verifying that metal cofactor saturation was

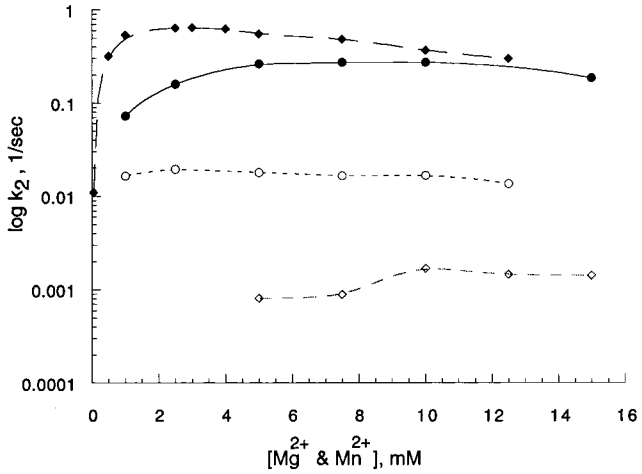

FIGURE 3: Plot of the logarithm of the single-turnover rate constant k_2 as a function of metal ion concentration for Mg^{2+} reactions (performed at pH 7.0) and Mn^{2+} reactions (performed at pH 6.5). Black diamonds and black circles depict data for wild-type reactions in the presence of Mn^{2+} and Mg^{2+}, respectively. White diamonds and white circles depict data for T93A reactions in the presence of Mg^{2+} and Mn^{2+}, respectively.

also attained near the upper bounds of the pH profiles (data not shown).

The pH−rate profiles of wild-type and T93A enzymes in the presence of Mg^{2+} each exhibit classic bell shapes (Figure 4A,B). Replots of the data on a logarithmic scale give slopes on the acidic limb of 0.90 for the wild type and 0.96 for T93A (Figure 5). On the basic limb, the values are 0.85 for the wild type and 0.87 for T93A. These slopes are each close to 1.0 and thus support a model for catalysis which requires two deprotonation steps for DNA cleavage. A striking feature of the profiles is the sharpness of the peaks and the absence of a pH-independent region at which the activities are maximal. This shows that the pK_a values for the ionizations must be separated by less than 2 pH units (*32*). The closeness of the pK_a's for the two ionizations places limits on the accuracy with which their actual values can be determined, and only the average of the two values can be precisely determined (*32*). However, we nevertheless attempted to fit the data for each enzyme to both eqs 1 and 2 using several strategies. First, the value for K_{max} in eq 1 was permitted to vary freely as a third independent variable in addition to the two pK_a's. For both wild-type and T93A enzymes, this produced a "reverse ionization" in which the value for pK_{a1} was higher than that of pK_{a2}, and the computed standard deviations were quite high (wild type, pK_{a1} = 9.40 ± 0.87 and pK_{a2} = 7.66 ± 0.85; T93A, pK_{a1} = 9.15 ± 0.37 and pK_{a2} = 8.50 ± 0.36). However, it was found that fixing K_{max} to certain values in eq 1 allowed much more accurate fitting as judged by reduced standard deviations. The best fits were obtained when K_{max} equaled 0.19 s^{-1} for T93A and when

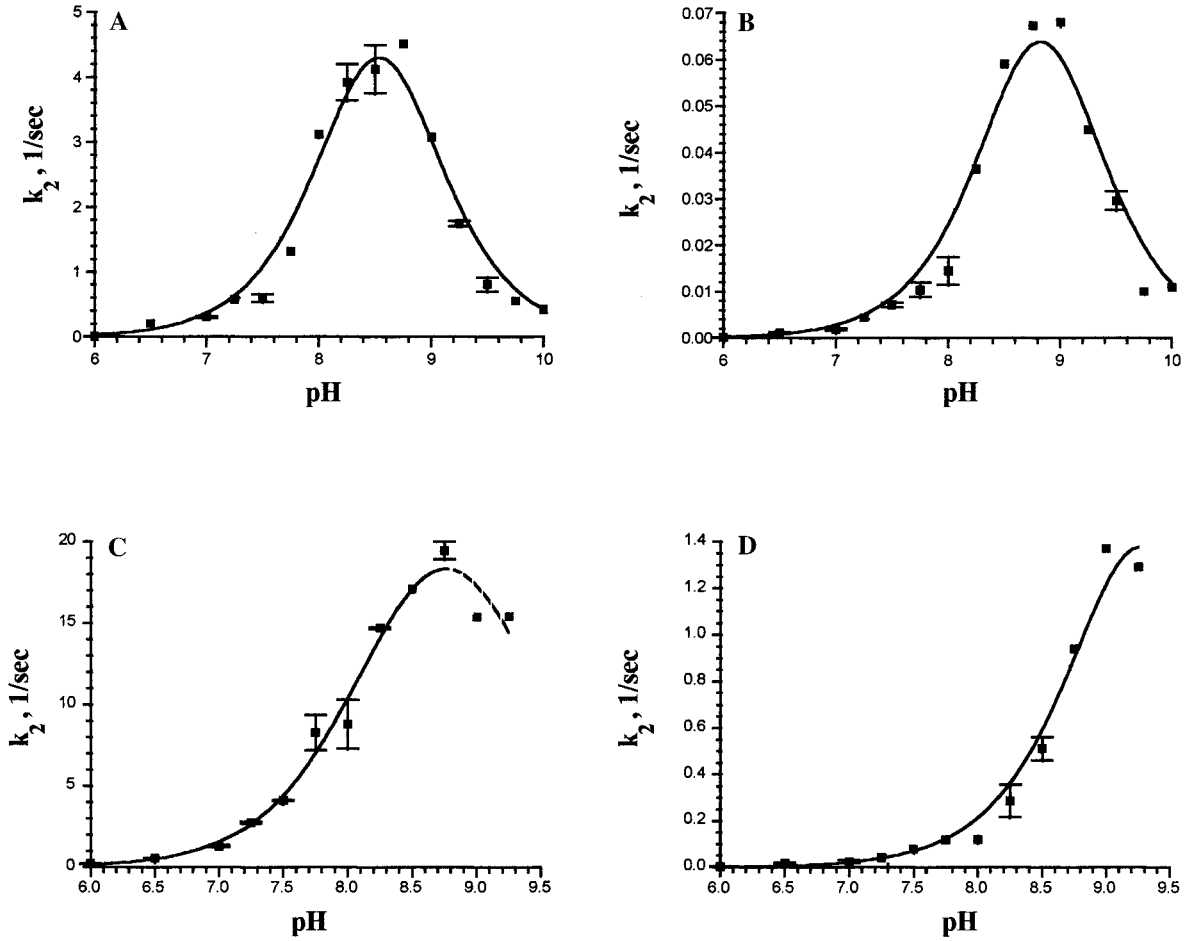

FIGURE 4: Plots of the single-turnover rate constant k_2 as a function of pH: (A) wild-type *Eco*RV reactions with the Mg^{2+} cofactor, (B) T93A reactions with the Mg^{2+} cofactor, (C) wild-type *Eco*RV reactions with the Mn^{2+} cofactor, and (D) T93A reactions with the Mn^{2+} cofactor. Error bars denote the standard deviations of the rate constants for reactions for which two or more independent measurements were taken. Data points for which no error bars are denoted represent single measurements at these pH values.

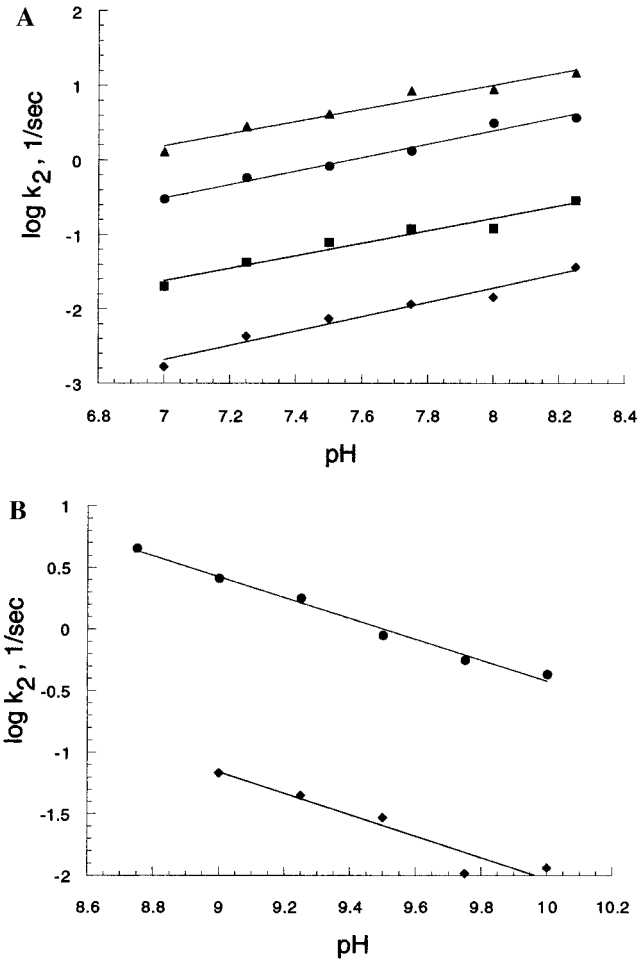

FIGURE 5: Log linear plots of the variation of the rate constant k_2 with pH. (A) Acidic limb of the profiles. Plotted are data for reactions of wild-type *Eco*RV with the Mn^{2+} cofactor (▲), wild-type *Eco*RV with the Mg^{2+} cofactor (●), T93A with the Mn^{2+} cofactor (■), and T93A with the Mg^{2+} cofactor (◆). (B) Basic limb of the pH profiles. Shown are data for the Mg^{2+}-dependent reactions of wild-type *Eco*RV (●) and T93A (◆).

K_{max} equaled 13.5 s^{-1} for the wild type; each of these values is 3-fold above the maximal rate at the peak of the respective profiles. At these K_{max} values, the pK_a values are as follows: wild type, pK_{a1} = 8.54 ± 0.04 and pK_{a2} = 8.52 ± 0.04; T93A, pK_{a1} = 8.82 ± 0.05 and pK_{a2} = 8.83 ± 0.04. For both enzymes, identical values with slightly higher standard deviations were obtained by fitting to eq 2 (while allowing K_{max} to vary independently). Because the absence of a flat top to the profiles indicates that the ionizations are less than 2 pH units apart, it is possible to state with confidence that pK_{a1} and pK_{a2} do not deviate by more than 1 pH unit from the precisely determined average values of 8.53 for the wild type and 8.82 for T93A. Clearly, the ionizations required for catalysis by the mutant enzyme are very similar to those required by the wild type.

The pH dependencies of phosphoryl transfer in the presence of Mn^{2+} are very similar in the acidic portion of the profiles, reaching a maximum value at pH 8.75 (wild type) and 9.0 (T93A mutant) (Figure 4C,D). Replots of the data on a logarithmic scale give slopes of 0.81 for the wild type and 0.83 for T93A (Figure 5), indicating a single deprotonation, as observed for Mg^{2+}. For both enzymes, the rate of catalysis slows as the pH is raised further, suggesting that similar bell-shaped profiles likely are obtained in these cases also. However, at pH ≥9.5, it was no longer possible to obtain accurate data because of the formation of insoluble precipitates of manganese oxide and manganese hydroxide (*35*). Although these precipitates do form at pH values of ≥8.0, the quality of the data in the range of pH 8.0−9.25 is not diminished (Figure 2C,D). Thus, we think it is likely that the measured rates are reliable, particularly since it is expected that the effect of the precipitation, if any, would be to decrease the speed of catalysis. Although the lack of data in the basic region precludes fitting to the equations describing a doubly ionizing system, it is clear from qualitative comparisons of the acidic regions that the ionization on this limb for Mn^{2+} reactions is similar to that for Mg^{2+} reactions. There is thus no significant metal cofactor dependence on the pK_a of the group which must be deprotonated for activity. Further, as in the case of Mg^{2+}-dependent catalysis, the T93A mutant again behaves in a manner nearly identical to that of the wild type.

As previously reported (*36*), for wild-type *Eco*RV the rate of phosphoryl transfer at pH 7.0 in the presence of Mn^{2+} is faster than the Mg^{2+}-promoted rate by approximately 4-fold. The T93A mutant exhibits a more pronounced cofactor effect, with Mn^{2+}-catalyzed phosphoryl transfer proceeding 15-fold faster than the Mg^{2+}-dependent reactions (Figure 4). At the pH where the rate is maximal (approximately 8.75), the wild-type enzyme catalyzes Mg^{2+}-dependent phosphoryl transfer approximately 65-fold faster than does T93A. The rate of the mutant is diminished only 20-fold in Mn^{2+}-catalyzed phosphoryl transfer, however, and at the optimal pH, the rate of Mn^{2+}-dependent DNA cleavage by T93A approaches to within 5-fold of the Mg^{2+}-dependent wild-type rate.

DISCUSSION

T93A Mutant as a Probe of Mechanism. An important objective of this study is to evaluate the suitability of T93A as a vehicle for elucidating the structural basis of catalysis. The impetus for this arises from our finding of a new divalent metal binding site in the active-site region, in the crystal structure of the *Eco*RV T93A−DNA−Ca^{2+} ternary complex. This site has not been observed in any wild-type structure of the enzyme−DNA complex. Instead, metal ions in wild-type structures bind to two other distinct sites, one of which is also occupied in T93A (Figure 1). Combining this information led to models for catalysis in which all three metals are incorporated, which are consistent with all available biochemical and mutagenesis data, and which require only very small adjustments in the positions of key groups for forming a pre-transition state ternary complex in which hydroxide ion is poised to attack at phosphorus (Figure 6). The detailed rationale for why mutually exclusive metal sites are observed in the wild-type and T93A mutant structures has been previously discussed (*15*).

The validity of the model rests in part on the assumption that T93A and wild-type *Eco*RV possess identical chemical mechanisms. This appeared to be reasonable on the basis of two previous observations: (i) the conformations of the active sites of T93A and the wild type are similar and (ii) the Mg^{2+}-dependent overall activity of T93A is preserved at 7% of the wild-type level as judged by k_{cat}/K_m values for a short oligodeoxynucleotide substrate (*33*). Additional and

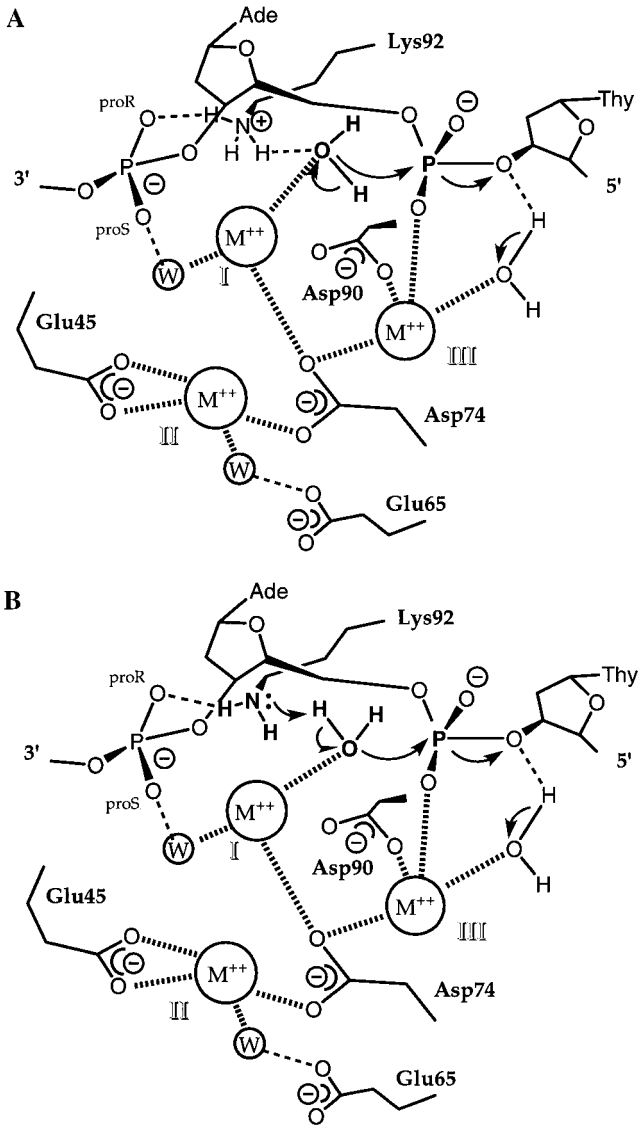

FIGURE 6: Alternative possibilities for the transition state of the metal ion-mediated DNA cleavage by *Eco*RV, each consistent with biochemical and crystallographic data. (A) A metal ion located in site I generates the attacking hydroxide nucleophile, which is stabilized and oriented by the positively charged Lys92. The proton is released to solvent or associates transiently with a DNA phosphate or active-site carboxylate group. (B) The same metal ion generates the attacking hydroxide, but Lys92 functions instead as a general base to accept the proton from water. Both mechanisms are based on combining information from the crystal structures of the wild-type and T93A enzymes (*15*).

more definitive evidence is provided by the pH−rate studies. The pH dependence of catalysis in the two enzymes is quite similar for both metal cofactors (Figures 4 and 5), with very similar bell-shaped curves and an observed shift of only 0.3 pH unit in the average value of the two closely adjacent pK_a's. Together with the high overall activity and the preservation of local active-site structure, these data offer very good evidence that the chemical mechanisms of the two enzymes are indeed the same.

The catalytic rates decreased 65-fold for Mg^{2+} reactions and 20-fold for Mn^{2+} reactions exhibited by T93A most likely arise from a small mispositioning of the reactive groups of the enzyme and DNA in the pre-transition state ternary complex. Much greater decreases would be expected if, for example, one or more of the metal ions were not bound by the mutant. Mispositioning is supported by the crystal structure of the T93A−DNA−Ca^{2+} complex, which shows that enzyme and DNA groups over a portion of the interface are shifted apart by roughly 1 Å even though their internal conformations are unchanged (*15*). It is also interesting to consider the structural basis for the 200-fold reduction in binding affinity (Table 1). In addition to the apparent weakening of some interactions at the enzyme−DNA interface, more global structural changes were observed in the T93A cocrystal structure and also in the structure of unliganded T93A (*12*, *15*). These encompass altered relative positions of rigid portions of the dimer, comprising the two catalytic/DNA binding domains and the dimer interface region. It thus appears that the decreased binding affinity may ultimately originate from differences in the induced-fit pathway, during which the DNA sharply bends and the protein undergoes numerous conformational changes en route to formation of a productive complex. Further analysis and experimentation with the T93A mutant is presently in progress. This is expected to provide additional insight into the details of the induced fit, particularly with respect to the roles of amino acids distant from the DNA binding cleft.

Structural Mechanism of Catalysis by EcoRV. The bell-shaped pH−rate profiles for wild-type and T93A enzymes in the presence of Mg^{2+} indicate the presence of two essential titratable groups in the enzyme−DNA−Mg^{2+} ternary complex. The maximal activity in the center of the pH range shows that the singly protonated form of the complex is catalytically active. Thus, the mechanism involves general base catalysis of the attack of hydroxide ion at the scissile phosphorus (pK_a = 8.53 ± 1.0) and general acid catalysis of the expulsion of the 3′-ribose hydroxyl group (pK_a = 8.53 ± 1.0). The large uncertainties in the estimate of each pK_a are a consequence of the fact that the values are within 2 pH units of each other. It is possible, therefore, that the pK_a of the base which deprotonates water is actually higher than that of the acid which protonates the leaving anion (*31*).

In addition to these pH studies, considerable other biochemical and crystallographic data of relevance to deducing the catalytic mechanism of *Eco*RV have been previously reported. Phosphorothioate modification experiments have shown that the reaction proceeds via an in-line attack by hydroxide which forms a transient pentacovalent transition-state species, with inversion of configuration (*5*). Thus, there is no stable covalent intermediate, and consideration can be limited to how the single trigonal bipyramidal transition state is stabilized. The reaction has an absolute requirement for divalent cations; for the preferred Mg^{2+} cofactor, it is well-established that at least two metals per enzyme subunit are required for cleavage (*8*, *9*). While Mg^{2+}-dependent overall rates are fastest, the rate of the chemical step of phosphoryl transfer is better catalyzed by Mn^{2+}, and the lower overall rates with this cofactor are caused by slower product release (*36*). Two of the metal binding sites located by X-ray studies are located between the crucial enzyme carboxylates Asp90 and Asp74, and the scissile and 3′-adjacent phosphates of the DNA (Figure 1 and sites I and III in Figure 6). Because neutralization of the phosphate charge is key to phosphodiester bond cleavage, the positions of these metals strongly suggest that they play a direct role in catalysis. It is also established that the enzyme residues most sensitive to mutation are Asp90, Asp74, and the directly adjacent Lys92

(Figure 6). Replacement of any of these side chains with alanine reduces the overall catalytic rate by 4−5 orders of magnitude (*17*).

A further important consideration in considering possible mechanisms is the reliability of the structural studies in providing a ground-state model from which the positions of key groups in the (experimentally unobservable) transition state may be deduced. For *Eco*RV, crystal structures of the cognate enzyme−DNA complex are available in five different crystal lattice environments (*10*, *11*; N. C. Horton and J. J. Perona, submitted for publication). All of these structures possess similar conformations for the active site and the DNA within the target site. Only small differences of 1.0−1.5 Å in the positions of the scissile phosphate and adjacent deoxyribose sugars are found. Significantly, catalytic activity is retained in one of these lattices (*10*; N. C. Horton and J. J. Perona, unpublished observations), suggesting that the observed ground-state conformation is similar to the transition state. Thus, it seems unlikely that the DNA undergoes considerable rearrangement prior to cleavage.

The three-metal ion mechanism we have proposed is consistent with the pH−rate profiles and all other biochemical data (*15*). In this mechanism (Figure 6A), the source of hydroxide ion is a water molecule bound in the inner sphere of a divalent metal ion. The metal is observed as Ca^{2+} in the cocrystal structure of the *Eco*RV T93A mutant bound to DNA (site I in Figure 6). It bridges through an inner sphere water molecule to the *pro*-S_P oxygen of the 3′-adjacent phosphate, explaining the low activity of the S_P-phosphorothioate derivative (*18*) as arising from disruption of this metal binding site. The other two metal sites observed in wild-type structures are also occupied in the model. The metal bound to the Asp90 and Asp74 carboxylates neutralizes the incipient negative charge in the pentacovalent transition state, and also provides an inner sphere water molecule which hydrogen bonds to the 3′-oxygen leaving group (site III in Figure 6). Ionization of this water promoted by the metal ion is used to protonate the leaving oxyanion. The metal in the 74/45 site (site II in Figure 6) plays a structural role in positioning Asp74. Only very small movements of the enzyme, the DNA, and the hydrated metals were needed to construct a plausible pre-transition state conformation, including all three metal ions (*15*; Figures 1 and 6).

We have previously discussed two possibilities for the critical role of Lys92 in promoting catalysis (*15*). In the first, the pK_a of the amine group (normally 10.5 in aqueous solution) is unshifted or is raised because of the proximity of the DNA phosphates and, in particular, the direct interaction with the *pro*-R_P oxygen of the 3′-adjacent phosphate (Figure 6A). The positively charged amine nitrogen then stabilizes the attacking water molecule and contributes to a further lowering of its pK_a. For Mg^{2+} as the metal cofactor, a pK_a value for the inner sphere water molecule of 11.4 is commonly used (*35*, and references therein), although values as high as 12.8 are reported in the literature (*37*). Analysis of the pH−rate profile indicates a general base with a pK_a of 8.5 ± 1.0 so that a shift of as little as 2 pH units may be required. A small shift of this magnitude is quite plausible due to the direct proximity of Lys92. The mechanism also invokes ionization of a metal-bound water for protonation of the 3′-leaving anion. This is in good accord with the pH studies as well, because the approximate equivalence observed for the two pK_a values is consistent with the same chemical event of metal-ligated water ionization being required for both general base and general acid catalysis. In addition, the finding that the rate of the chemical step is faster in the presence of Mn^{2+} (*36*; Table 1) is consistent with direct metal ligation to the scissile phosphate (Figure 6A,B), because the greater acidity of Mn^{2+} (as reflected in a lower pK_a for inner sphere waters) makes it better able to withdraw electrons from the P−O bond. Thus, the phosphorus is rendered more susceptible to nucleophilic attack by hydroxide ion.

This mechanism as proposed is poorly defined in the sense that the identity of the proton acceptor (the general base) is not explicitly indicated. Possibly, the proton is released to solvent or associates transiently with an adjacent carboxylate or phosphate group. An alternative possibility is that Lys92 in fact plays the role of the general base (Figure 6B). In this model, Lys92 and the hydrated metal ion operate in concert to provide highly efficient catalysis. This is quite plausible chemically, since the pK_a of 8.5 ± 1.0 for the general base requires a downward shift of only 2 pH units in the pK_a of the amine group, relative to its value in aqueous solution. However, a structural basis for the maintenance of Lys92 in the deprotonated state is less clear, in view of the adjacent negatively charged phosphates. Available approaches for the calculation of the pK_a's of active-site residues are not yet sufficiently accurate to permit an evaluation by theoretical means, particularly not in a system of this complexity (*38*). Further experimentation will be required to distinguish the two possibilities (Figure 6A,B).

The mechanisms depicted in Figure 6 position the two most important metal ions (sites I and III) in-line with the reaction trajectory, that is, on a line parallel with the apical positions of the trigonal bipyramid at phosphorus. Although there are differences in detail, this is an arrangement similar to that observed for the phosphoryl transfer reactions catalyzed by alkaline phosphatase (*20*) and by the 3′−5′ exonuclease active sites of *E. coli* DNA polymerase I (*19*) and T4 DNA polymerase (*21*). Recently, divalent metal ions have also been located in the active sites of type II restriction endonucleases *Bam*HI (*39*) and *Bgl*I (*40*) in their respective cocrystal structures with specific DNA. In both these cases as well, two metal ions are observed roughly in-line with the ligands at the apical positions of the scissile phosphates in the transition state. Further, for each of the enzymes (*Eco*RV, *Bam*HI, and *Bgl*I), a spatially conserved triad of charged amino acids (equivalent to Asp90, Asp74, and Lys92 of *Eco*RV) is located adjacent to the scissile phosphates and metal binding sites. The similarities observed among these three high-resolution structures in the same enzyme family provide some further confidence that the proposed *Eco*RV mechanisms depicted in Figure 6 may in fact obtain. While the crucial correlative kinetic data reported here and elsewhere for *Eco*RV are lacking for both *Bgl*I and *Bam*HI, the concordance of metal binding sites is nonetheless suggestive of a catalytic mechanism with many similar features among enzymes of the type II restriction endonuclease family. pH−rate studies have also been reported for *Eco*RI (*41*) and *Taq*I (*42*), in the latter case via single-turnover measurements of the chemical step. In *Taq*I, the Mg^{2+}-dependent rate increases in the pH range of 6.0−7.5 and remains constant from pH

7.5 to 8.75. Rates at higher pH values were not reported, leaving open the possibility of a bell-shaped profile as found for *Eco*RV. Should this be the case, the two ionizations would occur at more widely separated pH's than is observed here. The observation of only a single ionization is, however, consistent with a very similar mechanism in which a metal ion interacts directly with the 3′-leaving oxygen rather than through a water molecule. Such a direct interaction is indeed observed in *E. coli* alkaline phosphatase (*20*), in the 3′−5′ exonuclease active site of *E. coli* DNA polymerase I (*19*), in the *Bgl*I−DNA−Ca^{2+} ternary complex (*40*), and in the *Bam*HI−DNA−Ca^{2+} ternary complex (*39*).

Because the pH−rate data do not distinguish the identity of the ionizing groups, they should be viewed only as being consistent with the proposed mechanism. As a formal possibility, they are thus also consistent with the proposal that the *pro-*R_P oxygen of the 3′-adjacent phosphate is the catalytic base (*18*). However, the finding that a general base with a pK_a of 8.5 ± 1.0 deprotonates the water molecule makes it extremely unlikely that this is the case. This is because the pK_a of 1.5 for the phosphate oxygen of phosphodiesters in solution is now seen to impose a requirement for an upward shift of fully 6−8 orders of magnitude in proton affinity for this group, for it to function efficiently as the catalytic base. There are few to no well-documented examples of such a large shift for an ionizing group in any enzyme active site. Further, while the prediction of pK_a shifts based on inspection of crystal structures is hazardous, it is nonetheless the case that there are no uncompensated negatively charged groups located adjacent to the phosphate.

There have also been two related proposals for a two-metal ion mechanism for *Eco*RV in which the metals occupy sites II and III (Figure 6) (*8*, *11*). Unfortunately, both of these proposals require large rearrangements of the DNA relative to what is observed in the crystal structures. Further, a crucial role is suggested for Glu45, which is not consistent with the observation that the E45A mutant retains significantly more activity than do D74A or D90A (*17*). Moreover, in contrast to those of D74A and D90A, the activity of the E45A mutant can be significantly reconstituted in the presence of Mn^{2+} (*17*, *43*). Sigmoidal plots of reaction rate versus metal ion concentration, interpreted to mean that two or more metals are required for catalysis, have also been observed for E45A. This was taken as evidence for a distal metal binding site, since the 74/45 site would presumably be disrupted in the mutant. However, the sigmoidal plot is entirely consistent with the occupancy of sites I and III (neither of which involves Glu45) by metal ions in the E45A mutant, and thus with the mechanisms proposed here (Figure 6).

Conclusion. The bell-shaped pH−rate profile for *Eco*RV, showing a pH maximum of 8.5 and closely spaced pK_a's for the two ionizations, is entirely consistent with the three-metal ion mechanism for phosphoryl transfer proposed on the basis of crystal structures. The two closely related possibilities described here, which are distinguished by the protonation state of Lys92, best explain all of the available data acquired to date. However, it is desirable to discriminate between these, to further rule out other potential mechanisms, and to provide a more definitive crystallographic analysis perhaps not dependent on the combination of information from different structures. Additional and extensive experimentation for accomplishing these objectives is ongoing.

ACKNOWLEDGMENT

We thank Steven Halford for the gift of the T93A expression vector. We are grateful to Stan Parsons, Norbert Reich, Nancy Horton, and Amy Martin for assistance with data analysis and for ongoing discussions.

REFERENCES

1. Roberts, R. J., and Halford, S. E. (1993) in *Nucleases*, 2nd ed., pp 35−88, Cold Spring Harbor Laboratory Press, Plainview, NY.
2. Roberts, R. J., and Macelis, D. (1998) *Nucleic Acids Res. 26*, 338−350.
3. Gerlt, J. A. (1993) in *Nucleases*, 2nd ed., pp 1−34, Cold Spring Harbor Laboratory Press, Plainview, NY.
4. Connolly, B. A., Eckstein, F., and Pingoud, A. (1984) *J. Biol. Chem. 259*, 10760−10763.
5. Grasby, J. A., and Connolly, B. A. (1992) *Biochemistry 31*, 7855−7861.
6. Schildkraut, I., Banner, C. D. B., Rhodes, C. S., and Parekh, S. (1984) *Gene 27*, 327−329.
7. Vermote, C. L. M., and Halford, S. E. (1992) *Biochemistry 31*, 6082−6089.
8. Vipond, I. B., Baldwin, G. S., and Halford, S. E. (1995) *Biochemistry 34*, 697−704.
9. Baldwin, G. S., Vipond, I. B., and Halford, S. E. (1995) *Biochemistry 34*, 705−714.
10. Winkler, F. K., Banner, D. W., Oefner, C., Tsernoglou, T., Brown, R. S., Heathman, S. P., Bryan, R. K., Martin, P. D., Petratos, K., and Wilson, K. S. (1993) *EMBO J. 12*, 1781−1795.
11. Kostrewa, D., and Winkler, F. K. (1995) *Biochemistry 34*, 683−696.
12. Perona, J. J., and Martin, A. M. (1997) *J. Mol. Biol. 273*, 207−225.
13. Horton, N. C., and Perona, J. J. (1998) *J. Mol. Biol. 277*, 779−787.
14. Horton, N. C., and Perona, J. J. (1998) *J. Biol. Chem. 273*, 21721−21729.
15. Horton, N. C., Newberry, K. J., and Perona, J. J. (1998) *Proc. Natl. Acad. Sci. U.S.A. 95*, 13489−13494.
16. Martin, A. M., Sam, M. D., Reich, N. O., and Perona, J. J. (1999) *Nat. Struct. Biol. 6*, 269−277.
17. Selent, U., Ruter, T., Kohler, E., Liedtke, M., Thielking, V., Alves, J., Oelgeschlager, T., Wolfes, H., Peters, F., and Pingoud, A. (1992) *Biochemistry 31*, 4808−4815.
18. Jeltsch, A., Alves, A., Wolfes, H., Maass, G., and Pingoud, A. (1993) *Proc. Natl. Acad. Sci. U.S.A. 90*, 8499−8503.
19. Beese, L. J., and Steitz, T. A. (1991) *EMBO J. 10*, 25−33.
20. Kim, E. E., and Wyckoff, H. W. (1991) *J. Mol. Biol. 218*, 449−464.
21. Wang, J., Yu, P., Lin, T. C., Konigsberg, W. H., and Steitz, T. A. (1996) *Biochemistry 35*, 8110−8119.
22. Vipond, I. B., and Halford, S. E. (1995) *Biochemistry 34*, 1113−1119.
23. Knowles, J. R. (1976) *CRC Crit. Rev. Biochem. 4*, 165−172.
24. Vermote, C. L. M., Vipond, I. B., and Halford, S. E. (1992) *Biochemistry 31*, 6089−6097.
25. Vipond, I. B., and Halford, S. E. (1996) *Biochemistry 35*, 1701−1711.
26. Luke, P. A., McCallum, S. A., and Halford, S. E. (1987) *Gene Amplif. Anal. 5*, 183−205.
27. Aggarwal, A. K. (1990) *Methods: A Companion to Methods in Enzymology 1*, 83−90.
28. Carey, J. (1991) *Methods Enzymol. 208*, 103−117.
29. Engler, L. E., Welch, K. K., and Jen-Jacobson, L. (1997) *J. Mol. Biol. 269*, 82−101.
30. Fersht, A. R. (1985) *Enzyme Structure and Mechanism*, 2nd ed., W. H. Freeman & Co., New York.
31. Cleland, W. W. (1977) *Adv. Enzymol. 45*, 273−387.

32. Cleland, W. W. (1990) Steady-State Kinetics, *The Enzymes (3rd Ed.) 19*, 99−158.
33. Wenz, C., Jeltsch, A., and Pingoud, A. (1996) *J. Biol. Chem. 271*, 5565−5573.
34. Lagunavicius, A., and Siksnys, V. (1997) *Biochemistry 36*, 11086−11092.
35. Dahm, S. C., Derrick, W. B., and Uhlenbeck, O. C. (1993) *Biochemistry 32*, 13040−13045.
36. Sam, M. D., and Perona, J. J. (1999) *J. Am. Chem. Soc. 121*, 1444−1447.
37. Chabarek, S., Courtney, R. C., and Martell, A. E. (1952) *J. Am. Chem. Soc. 74*, 5057.
38. Sham, Y. Y., Chu, Z. T., and Warshel, A. (1997) *J. Phys. Chem. B 101*, 4458−4472.
39. Viadiu, H., and Aggarwal, A. K. (1998) *Nat. Struct. Biol. 5*, 910.
40. Newman, M., Lunnen, K., Wilson, G., Greci, J., Schildkraut, I., and Phillips, S. E. V. (1998) *EMBO J. 17*, 5466.
41. Jeltsch, A., Alves, J., Oelgeschlager, T., Wolfes, H., Maass, G., and Pingoud, A. (1993) *J. Mol. Biol. 229*, 221−234.
42. Zebala, J. A., Choi, J., and Barany, F. (1992) *J. Biol. Chem. 267*, 8097−8105.
43. Groll, D. H., Jeltsch, A., Selent, U., and Pingoud, A. (1997) *Biochemistry 36*, 11389−11401.
44. Martin, A. M., Horton, N. C., Lusetti, S. L., Reich, N. D., and Perona, J. J. (1999) *Biochemistry* (in press).

BI9901580